FUNDAMENTAL ASPECTS OF GAS-LIQUID FLOWS

Edited by
E. E. MICHAELIDES

FED-Vol. 29

FUNDAMENTAL ASPECTS OF GAS–LIQUID FLOWS

presented at

THE WINTER ANNUAL MEETING OF
THE AMERICAN SOCIETY OF MECHANICAL ENGINEERS
MIAMI BEACH, FLORIDA
NOVEMBER 17–22, 1985

sponsored by

THE FLUIDS ENGINEERING DIVISION, ASME

edited by

E.E. MICHAELIDES
UNIVERSITY OF DELAWARE

THE AMERICAN SOCIETY OF MECHANICAL ENGINEERS
United Engineering Center 345 East 47th Street New York, N.Y. 10017

Library of Congress Catalog Card Number 85-73077

FOREWORD

This volume contains papers presented at the ASME 1985 Winter Annual Meeting in the International Symposium "Fundamental Aspects of Gas-Liquid Flows" sponsored by the Multiphase Flow Committee, Fluids Engineering Division. In the Last two decades the number of research projects on Gas-Liquid Flows has increased dramatically. New experimental techniques, modeling and numerical methods have been developed to solve the multitude of problems associated with these complex flows. The papers in this volume are representative of the recent advances in the area of Gas-Liquid Flows. They emanate from scientific projects in nine of the worlds leading industrial countries, and they all bring new insight into complex phenomena.

The theme of the symposium is general and the papers presented reflect this generality. For the purpose of presentation it was necessary to divide the papers into five sessions of two hours duration each. Each session covers a variety of topics:

The first session contains papers on the effect of pipe fittings on the thermal hydraulics of two-phase flows, transitions of flow regimes and an experimental method of void fraction measurements.

In the second session the first two papers are experimental; the next two papers pertain to the rise of gas and water slugs, while the last paper presents new modeling for the champaign effect.

Boiling and condensation are the topics of the first three papers in the third session. The rest are on the maximum size of bubbles and drops and the modeling of flashing flows.

The fourth session starts with a paper on turbulence in bubbly flows: the stability for the equations of the two-fluid model is discussed in the second paper. Bubbly flows is the theme of the next three papers as they pertain to water aeration, cavitation and water hammer phenomena.

The fifth and final session contains papers on critical flow through small breaks and two-phase flow instabilities.

The papers in this volume represent an encouraging transition in the two-phase flow literature from simple correlative approaches to more basic understanding of the phenomena and more detailed modeling. This trend, observed in the recent years is believed to bring us closer to the solution of fundamental problems and eventually to better design of components and plants.

Many scientists helped in the organization and running of this symposium. I am greatly indebted to all. In particular I would like to express my thanks to the members of the organizing committee, Drs. J. H. Kim, O. A. Arnas, O. Furuya, and U. S. Rohatgi, the Chairmen and Vice-Chairmen of the Symposium, the authors of the papers and the paper reviewers.

E. E. Michaelides
Symposium Chairman

CONTENTS

THERMAL HYDRAULICS OF A FEED-WATER PIPE BREAKAGE WITH A BACK-PRESSURE CHECK VALVE

J. R. Travis and M. D. Torrey
Theoretical Division, Group T-3
University of California
Los Alamos National Laboratory
Los Alamos, New Mexico

ABSTRACT

The SOLA-LOOP computer code for transient, non-equilibrium, two-phase flows in networks has been coupled with a dynamic check valve model. Transient back-pressure check valve behavior and fluid dynamic effects in the form of the so called water-hammer are numerically simulated for a feed-water pipe breakage accident. Three tests from the Superheated Steam Reactor Safety Program Project (PHDR) carried out near Frankfurt, West Germany are analyzed, and the calculated transient back-pressure check valve behavior and fluid dynamics effects are found to be in excellent agreement with the experimentally measured data.

NOMENCLATURE

A	Area
C	Mass exchange coefficient
C_D	Hydraulic damping coefficient
C_{VH}	Valve head resistance coefficient
D_K	Valve head diameter
D_s	Valve spindle diameter
F	Force on the valve
f_{vis}	Form and wall friction losses
g	Gravitational constant
I	Specific internal energy
K_1	Spring constant
K_2	External force
M	Mass of valve moving parts
P	Pressure
t	Time
u	Velocity
V	Fluid velocity upstream of valve
W_{vis}	Energy dissipation
x	Valve position
y	Axial position
Γ	Mass exchange function
ξ_K	Valve head resistance coefficient
ξ_v	Valve flow loss coefficient
ρ	Density

Subscripts

D	Downstream of valve head
ℓ	Liquid
s	Saturation
u	Upstream of valve head
v	Vapor
1	Pressure force
2	Hydraulic damping force
3	Spring force
4	Gravitational force

INTRODUCTION

Should a feed-water pipe in a nuclear power plant break, the feed-water back-pressure check valve has the function of limiting the loss of coolant. The check valve must close quickly, with the result that the escaping fluid comes to rest in a very short period of time. Forces are developed in the pipe by the rapid closure of the valve that may lead to stresses of considerable magnitude on the valve, piping system, and pipe supports. The so-called "fast-slow" feed-water back-pressure check valves have been designed to solve this problem. These valves have an optimized damping mechanism so that the last part of the closure stroke is very slow, thus minimizing the water-hammer effects.

An experimental performance analysis has been conducted (1) by the PHDR of the Kernforschungszentrum near Frankfurt, West Germany, utilizing a full scale previously operational single loop pressurized water reactor facility. The German blowdown experiments, with which we are to compare the SOLA-LOOP (2) calculated results, consisted of three tests. It was the objective of these tests to investigate the closure of the feed-water back-pressure check valve and the fluid dynamics in the piping network following a sudden pipe rupture.

EXPERIMENTAL FACILITY

The pipe system used for the blowdown experiments, including the auxiliary devices, is shown in Fig. 1. The steady state flow path, which is depicted by arrows on the figure, leads from the S-connector (3) of the reactor pressure vessel (1) through a ball-shaped

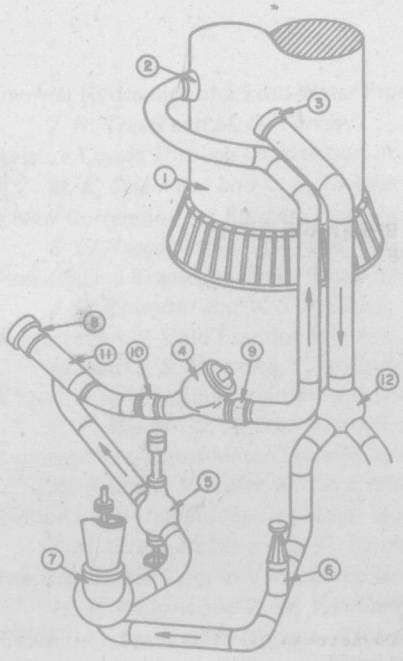

1 Reactor pressure tank (RPT)
2 T-connector
3 S-connector
4 Experimental valve
5 Quick-action stop valve
6 Shut-off gate valve
7 Circulation pump
8 Rupture connector
9 Measuring ring I
10 Measuring ring II
11 Measuring ring III
12 T-fitting
13 Ball fitting

Fig. 1. Experimental pipe system (from Ref. 1). The steady state flow path is shown by the arrows on the pipe centerline.

fitting (13), the suction-side shut-off gate valve (6), the circulation pump (7), the quick-action stop valve (5), the T-fitting (12), the measuring ring II (10), the experimental check valve (4), and measuring ring I (9) back to the reactor pressure tank (1). On the other side of the T-filling (12), the rupture connector (8) connects with the rupture disk device and the measuring ring III (11).

At the initialization of the flow conditions, the circulation pump establishes a flow rate of approximately 1600 m^3/h, which corresponds to an average steady state flow velocity of roughly 4.0 m/s in the pipe loop. At the moment the rupture disks break, the circulation pump (7) is shut off, and the quick-action stop valve (5) has the function of closing off the S-loop in about 1 s. As a further shut-off device in the S-loop, there is also a shut-off gate valve (6) which takes about 2 min to close.

To initiate the blowdown, the pressure between the two rupture disks is raised quickly so that the outer disk is blown out the end of the pipe. This results in a large pressure differential across the inner rupture disk and it is also blown out. The pipe cross-section is completely opened within 3 ms.

The experimental valve is a feed-water back-pressure check valve with hydraulic end damping. Figure 2 shows the check valve in the horizontal plane of the pipe axis as it is installed in the experimental superheated steam reactor plant. The valve apparatus is installed in the housing at an angle of 45 degrees, with the movable valve head (H) and the damping piston (D) both rigidly connected to the spindle (S).

Upon blowdown, the normal flow shown in Fig. 2 from left to right is reversed and the valve head moves from the open position shown to the closed position with the valve head seating in the valve throat. This motion is at first fast but in its final phase much slower as damping begins as soon as the annular gap between the cylinder and the damping piston narrows to a small width as the damping piston lowers. Figure 3 shows the damping design with the gentle taper between the larger cylindrical diameter (very little damping) to the smaller cylindrical diameter (maximum damping). The valve head closing rate depends on the resistance the annular gap presents to the flow of water from the chamber under the piston. For experiments V60.1 and V60.2 the annular gap is 0.3 mm, and experiment V60.3

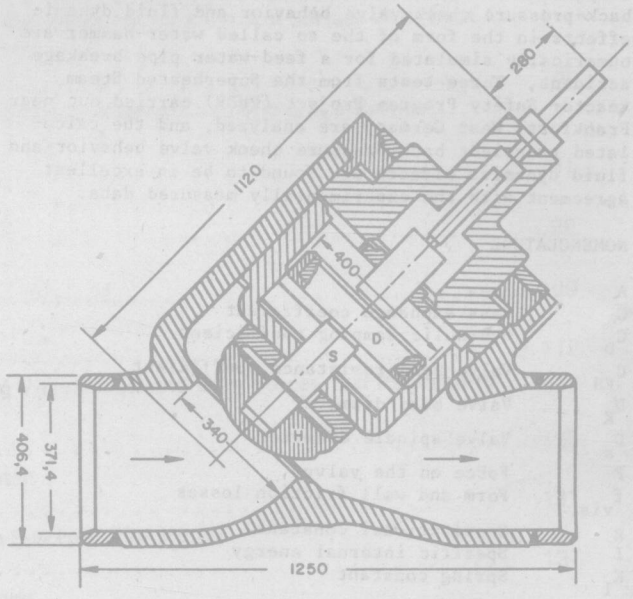

Fig. 2. Back-pressure experimental check valve (from Ref. 1). The steady state flow path is shown by the arrows. Dimensions are given in millimeters.

has an annular gap equal to 1.3 mm. Less flow resistance, for example, can be designed into the damping phase by increasing the annular gap width or by decreasing the roughness of the annular surfaces.

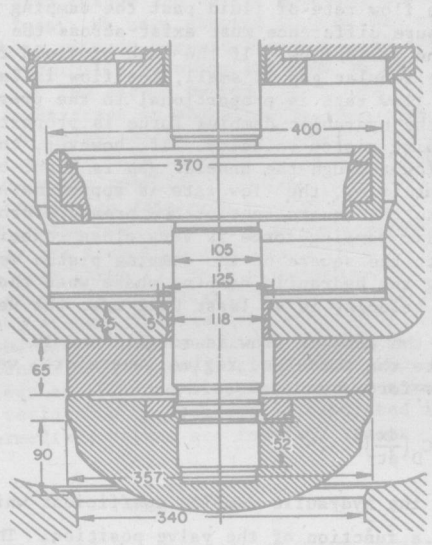

Fig. 3. Valve head, damping-piston, and damping chamber (from Ref. 1). Dimensions are given in millimeters.

DESCRIPTION OF THE THEORETICAL MODEL

The SOLA-LOOP (2) computer code has been utilized to calculate the flow in the pipe network shown in Fig. 1. SOLA-LOOP is a sophisticated yet fairly simple, very user friendly, highly flexible computer code for transient, nonequilibrium, two-phase flow in networks. Each component may have a one-dimensional representation with variable cross-sectional area. The flow dynamics is governed by a set of nonlinear conservation laws based on a generalized drift-flux model for two-phase mixtures. The equations are solved by a partially implicit finite-difference method [ICE: Implicit Continuous-fluid Eulerian (3)] that can use different time steps in different components. The complete equations and constitutive relations describing interphase transfers of mass, momentum, and energy, as well as the details of the numerical solution technique can be found in Ref. 2. For the purposes of this paper, only a brief sketch of a reduced form of these equations is given here.

At the flow rates of interest, it is anticipated that the relative velocity between phases will be small. Therefore, for this discussion we assume that the two phases comprising the fluid mixture move with the same average velocity.

In the case of equal phase velocities (mechanical equilibrium) and equal phase temperatures (thermal equilibrium), the governing equations for the two phase mixture density, ρ, velocity, u, and internal energy, I, reduce to

$$\frac{\partial \rho}{\partial t} + \frac{1}{A}\frac{\partial}{\partial y}(A\rho u) = 0 \quad , \tag{1}$$

$$\frac{\partial \rho u}{\partial t} + \frac{1}{A}\frac{\partial}{\partial y}(A\rho u^2) = -\frac{\partial P}{\partial y} + f_{vis} \quad , \tag{2}$$

$$\frac{\partial \rho I}{\partial t} + \frac{1}{A}\frac{\partial}{\partial y}(A\rho I u) = -\frac{P}{A}\frac{\partial}{\partial y}(Au) + W_{vis} \quad , \tag{3}$$

where A is the time-independent, cross-sectional area of the flow channel or pipe. Local flow losses from rapid area changes are accounted for by adding the necessary pressure loss and energy dissipation to Eqs. (2) and (3) through the terms f_{vis} and W_{vis}, respectively. In addition, the term f_{vis} accounts for pressure losses due to pipe wall friction. These equations must be supplemented with an equation for the macroscopic vapor density, ρ_v,

$$\frac{\partial \rho_v}{\partial t} + \frac{1}{A}\frac{\partial}{\partial y}(A\rho_v u) = \Gamma \quad , \tag{4}$$

where Γ is the rate of production of vapor mass per unit volume and time. For the present study, we have assumed that the vapor and liquid temperatures are both equal to the saturation temperature (thermal equilibrium). This is accomplished by choosing a vapor production rate of the form

$$\Gamma = C(T_\ell - T_s) \quad , \tag{5}$$

where T_ℓ and T_s are the liquid and saturation temperatures, respectively. The coefficient, C, is set sufficiently large, of the order 10^4 kg/m^3·s·K, to insure a large enough vapor production rate to produce nearly continuous equilibrium states in which the temperatures of liquid, gas, and saturation are the same. This development leads to what is commonly called the homogeneous equilibrium model (HEM).

In order to include the dynamical effect of the back-pressure check valve on the fluid dynamics, it is necessary to couple a valve model to SOLA-LOOP. This coupling is accomplished with SOLA-LOOP supplying time-dependent fluid velocities, densities, and pressures to the valve model, and in return, the valve model calculates a time-dependent valve head position (stroke), which is used to determine the resistance to flow through the valve. The equilibrium of forces on the valve head is established by the acceleration, the pressure force of the fluid, the damping force of the valve, the gravitational force, as well as any external actuating force and/or spring support of the movement of the valve. This force balance for the valve used in these experiments can be written as

$$m\frac{d^2x}{dt^2} = \sum_{i=1}^{4} F \quad , \tag{6}$$

where the indices depict the following forces:

(1) Pressure Force

$$F_1 = -P_u \cdot A_u + P_D \cdot A_D - C_{VH} \cdot A_u \cdot \frac{\rho}{2} \cdot V^2 \tag{7}$$

where

P_u = the pressure upstream of the valve head,

A_u = the upstream valve head area,
P_D = the pressure downstream of the valve head,
A_D = the downstream valve head area,
C_{VH} = the resistance coefficient of the valve head,
ρ = the fluid density, and
V = the fluid velocity upstream of the valve.

The actual pressure force is an integration of the three-dimensional pressure distribution over the valve head. Since P_u and P_D are only average upstream and downstream pressures respectively, a correction is applied effectively in the form of the third term to account for actual three-dimensional pressure variations around the valve head. This term is sometimes thought of as the flow resistance, and therefore, the non-dimensional coefficient C_{VH} is often called the valve head resistance coefficient. This coefficient is expressed as

$$C_{VH} = \frac{10^3}{\rho} \xi_K \quad , \tag{8}$$

where ξ_K is tabulated in Ref. 4, and also listed in Table I as a function of the valve head position. Any intermediate values may be found by linear interpolation of those listed in the table. The upstream valve head area is the valve head area minus the cross sectional area of the valve spindle,

$$A_u = \frac{\pi}{4} \left(D_K^2 - D_s^2\right) \quad , \tag{9}$$

where the outer valve head diameter, D_K = 357 mm, and the spindle diameter, D_s = 105 mm; thus A_u = 0.0914 m^2, and the downstream valve head area is

$$A_D = \frac{\pi}{4} D_K^2 = 0.1 \ m^2 \quad . \tag{10}$$

The pressures, P_u and P_D, the fluid velocity, V, and the fluid density, ρ, are supplied by the fluid dynamics module, SOLA-LOOP.

TABLE I

VALVE HEAD RESISTANCE COEFFICIENT AS A FUNCTION OF VALVE HEAD POSITION (FROM REF. 4)

Valve Head Position (mm)	Valve Head Resistance Coefficient ξ_K
130.0	0.0*
90.0	0.054
70.0	0.74
40.0	21.4
13.125	87.8
6.875	161.0
0.0	1548.8*

* Valve head resistance coefficient values were determined by extrapolating the data in Ref. 4.

(2) Hydraulic Damping Force

Motion between the damping piston and the cylinder is resisted by the fluid because the fluid must move from one side of the piston to the other through the annular gap. The greater the velocity, the greater must be the flow rate of fluid past the damping piston and a pressure difference must exist across the piston to cause the fluid flow. If the rate of fluid flow through the annular gap is small, the flow is laminar (i.e., the flow rate is proportional to the pressure drop) and the hydraulic damping force is proportional to the damping piston velocity. If, however, the rate of fluid flow through the annular gap is high, the flow is turbulent (i.e., the flow rate is approximately proportional to the square root of the pressure drop) and the hydraulic damping force is very close to being proportional to the square of the damping piston velocity. During the hydraulic damping phase when the damping piston velocity is at least 0.12 m/s, the Reynolds number for the annular flow is roughly 8×10^5, which is well into the turbulent regime; therefore, we represent this force by

$$F_2 = C_D \left(\frac{dx}{dt}\right)^2 \quad , \tag{11}$$

where C_D = the hydraulic damping coefficient which is in general a function of the valve position. This coefficient will be discussed in more detail in the next section.

(3) External Actuating Force and/or Spring Force

$$F_3 = - K_1 \cdot (x - x_1) - K_2 \tag{12}$$

where

K_1 = the linear spring constant,
x_1 = the position of zero, spring force, and
K_2 = any constant external force.

The spring constant, K_1, equals 1484 N/m, and the position of zero spring force, x_1, is 0.15 m. In order to compare with the early time ($t < 0.05$ s) valve position closure data, which will be discussed in the next section, it was necessary to set K_2 = 3000 N.

(4) Gravitational Force

$$F_4 = -m \cdot g \cdot \cos (45°) \tag{13}$$

where

m = the mass of the movable valve mechanism (190 Kg),

and

g = acceleration due to gravity (981 m/s^2).

The dynamical behavior of the check valve influences the fluid dynamics through a pressure loss in the f_{vis} term in Eq. (2). This pressure loss is represented, $\Delta p = \xi_v \left(\frac{1}{2} \rho V^2\right)$, where ρ and V are the upstream fluid density and velocity, respectively, and ξ_v is the valve position dependent flow loss coefficient. There are two ways of accounting for this pressure loss. The

first is to sum the effects of actually changing the area open to flow in the mesh cell representing the valve and adding a pressure loss such that the total loss from the time dependent area change plus the added pressure loss equals the desired total pressure loss. The second method is to derive the same pressure loss by ignoring the area change and simply modeling a functional pressure loss. We have elected to make use of the second of these methods because the numerical loss associated with physically changing the area is not well known, and for the second method, it is simply a matter of being consistant in choosing the flow loss coefficient and velocity position. Reference 4 lists steady state values for this resistance coefficient as a function of the valve position or stroke. We have found in comparisons with data from the three experiments discussed in the next section that these steady state resistances are less than what are actually needed. It has been shown (5) that with decelerating flows, the resistance is appreciably more than for the equivalent steady state. This is consistent with our findings, and therefore, has lead us to develop our own position dependent flow loss coefficient based upon the unsteady transient experiments discussed in the next section. This resistance coefficient is tabulated in Table II. Intermediate values are found by linear interpolation.

TABLE II

FLOW LOSS COEFFICIENT AS A FUNCTION OF VALVE POSITION

Valve Position (mm)	Flow Loss Coefficient, ξ_v
0.0	2.0×10^7
10^{-5}	7.5×10^6
10^{-4}	2.0×10^6
10^{-3}	3.0×10^5
10^{-2}	6.0×10^4
10^{-1}	1.2×10^4
1	2.5×10^3
5	9.0×10^2
10	5.5×10^2
20	3.2×10^2
30	2.22×10^2
40	1.45×10^2
50	1.0×10^2
60	5.0×10^1
70	2.2×10^1
80	10.0
130	2.0

EXPERIMENTAL AND COMPUTATIONAL RESULTS

The test parameters for the three tests are as follows:

V60.1 - Test with normal BWR - design conditions and with near optimized damping in the check valve.

V60.2 - Test with the same check valve damping as in V60.1 but with stronger thermodynamic conditions due to the cold water in the test pipe.

V60.3 - Test with normal BWR - design conditions but with reduced damping in the check valve.

The boundary and initial conditions are:

length of the test pipe	:	15.0 m
diameter of the test pipe	:	371.4 mm
diameter of the rupture nozzle	:	453.0 mm
pressure in the vessel	:	70.0 bar
temperature in the vessel	:	285.0°C
temperature in the pipe		
V60.1 and V60.3	:	220.0°C
V60.2	:	50.0°C
valve position	:	88.0 mm
velocity in pipe	:	4.0 m/s

In Figs. 4, 5, and 6, the time history of the valve position, there is an undamped run from the initial position to roughly 75 mm. At that time (approximately 0.03 s) the annular gap has decreased so that hydraulic damping becomes important. This is evidenced by the dramatic change in the slope of the closing curves, at least in tests V60.1 and V60.2, in which the valve design attempted to soften or minimize the water-hammer effect. In test V60.3 the closure rate is largely unaffected by damping, although it is noted that there is a slight slope change at 75 mm or 0.03 s as well. As the valve continues to close, there is another change in the closing curve slope for V60.1 and V60.2 at approximately 55 mm (0.15 s) or just before the curves become linear. For V60.3 the linear portion of the closing curve does not start until the valve has closed to about 45 mm or roughly 0.1 s. Reference 1 lists the closing times of 605 ms, 594 ms, and 145 ms for V60.1, V60.2, and V60.3, respectively. In these comparisons and the ones to follow, the calculated curves are designated with triangles while the measured experimental data are shown unmarked.

In order that the calculated valve closing curve match the experimental curve, the damping coefficient, C_D, was adjusted for the three experiments as shown in Table III. Valve position values between 40.0 mm, 60.0 mm, and 75.0 mm were evaluated by linear interpolation.

Pressure histories just upstream of the valve for the three experiments and calculations are presented in Figs. 7, 8, and 9. The rather sharp pressure spike at 0.03 s for all three experiments is a result of the change in the closing curve slope at that time. Additionally, there are local pressure maxima corresponding in time to the other closing curve slopes changes, namely 0.15 s for V60.1 (Fig. 7) and V60.2 (Fig. 8) and 0.1 s for V60.3 (Fig. 9). Through the linear portion of the closing curve until the valve is actually closed, there is relatively very little pressure change; however, after closing, the water-hammer effect is dramatically shown in all three experiments. For tests V60.1 (Fig. 7) and V60.2 (Fig. 8), this water-hammer is in the neighborhood of 10 - 15 bars, while in V60.3, where the closure rate is largely unaffected by hydraulic damping, and consequently, the water-hammer is very pronounced and closer to 70 bars. The water-hammer or 1/4 period pressure waves are set up in the isolated pipe between the closed valve and the pressure vessel. These waves are shown to decay in time. Pressure histories on the downstream side of the valve are presented in Figs. 10, 11, and 12. After the initial transient of roughly 0.1 s, the first closing curve change of slope is reflected in the sharp spike at 0.03 s, the pressures quickly approach their saturated values corresponding to the liquid temperature. Mass

flow rate measurements at measuring ring I (Figs. 13, 14, and 15) exhibit an initial fluid acceleration through the valve (times < 0.1 s) and then deceleration as the flow resistance increases corresponding to the valve closing.

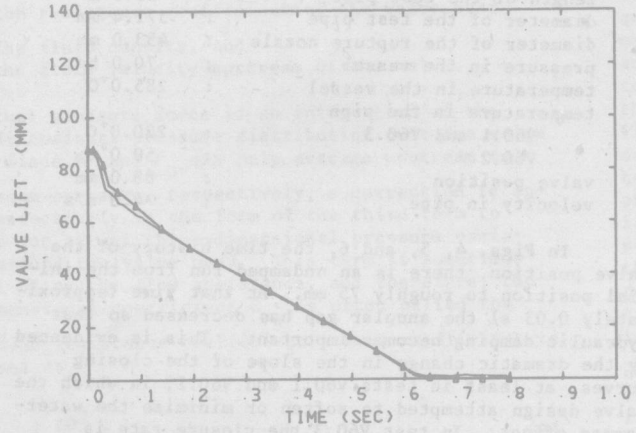

Fig. 4. Valve position for V60.1. Calculated results are shown with triangles.

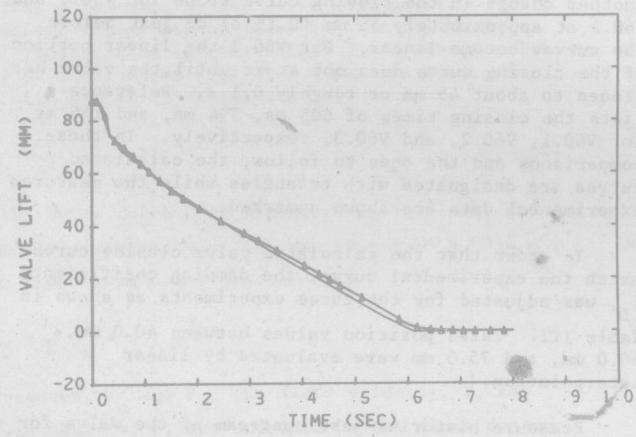

Fig. 5. Valve position for V60.2. Calculated results are shown with triangles.

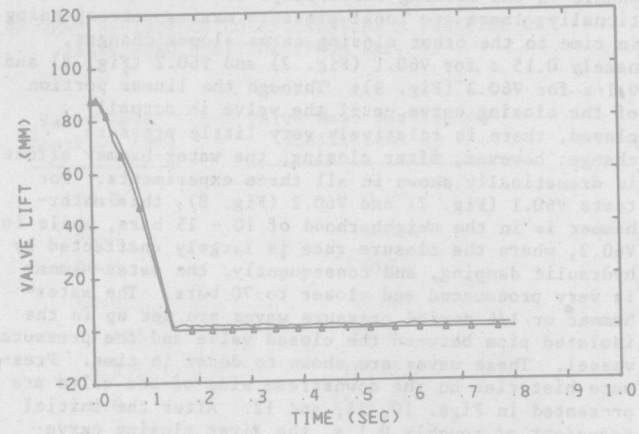

Fig. 6. Valve position for V60.3. Calculated results are shown with triangles.

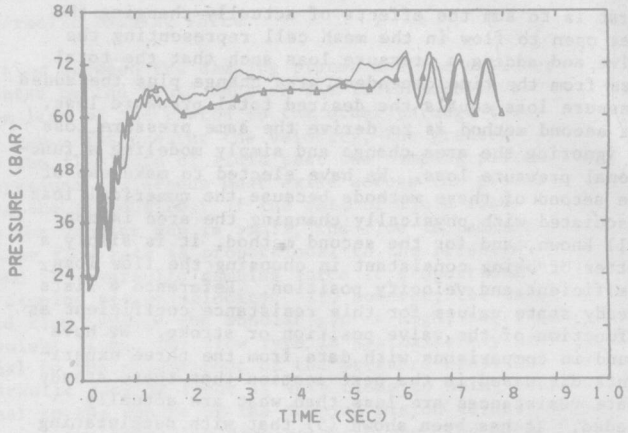

Fig. 7. Pressure upstream of valve for V60.1. Calculated results are shown with triangles.

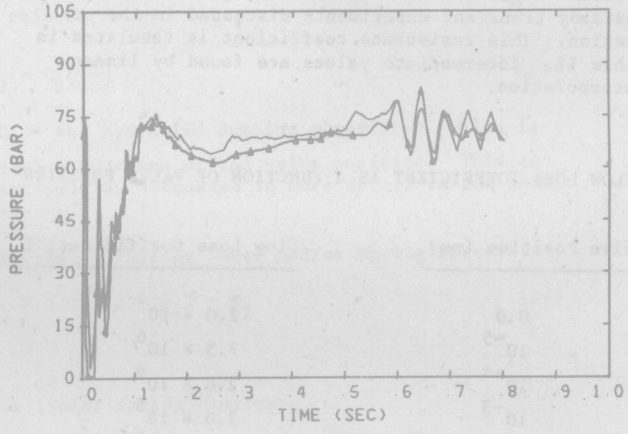

Fig. 8. Pressure upstream of valve for V60.2. Calculated results are shown with triangles.

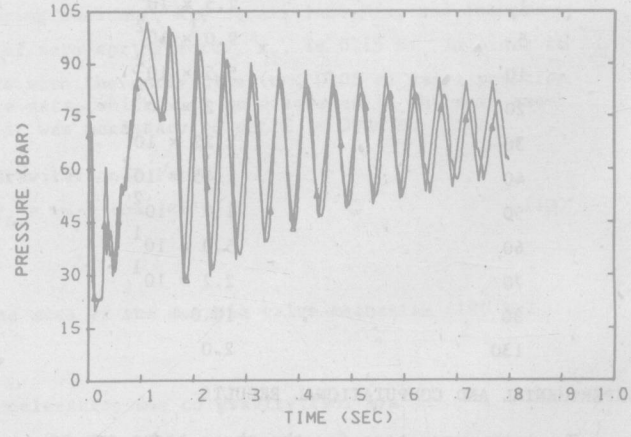

Fig. 9. Pressure upstream of valve for V60.3. Calculated results are shown with triangles.

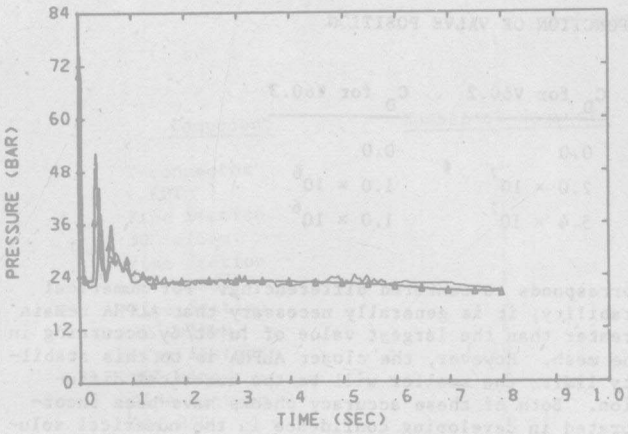

Fig. 10. Pressure downstream of valve for V60.1. Calculated results are shown with triangles.

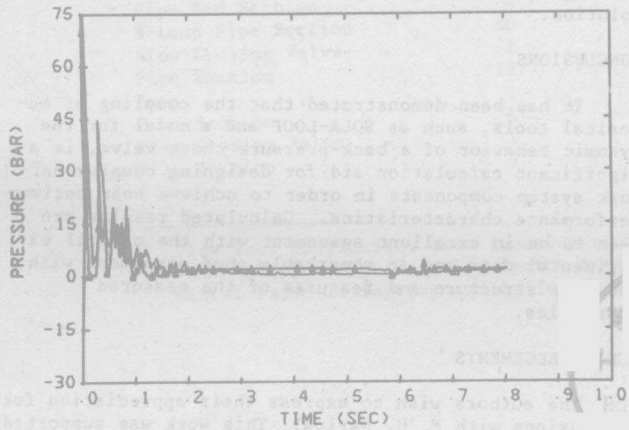

Fig. 11. Pressure downstream of valve for V60.2. Calculated results are shown with triangles.

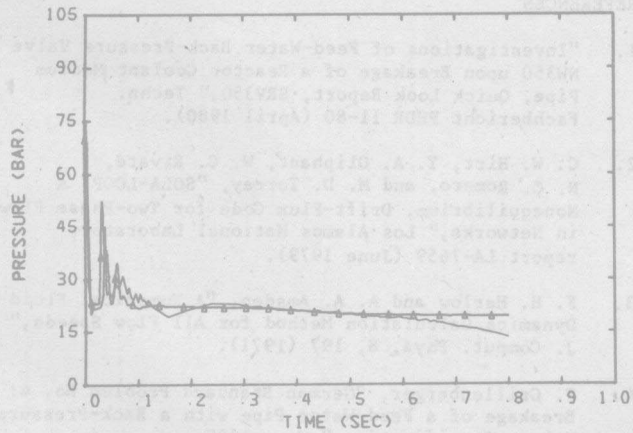

Fig. 12. Pressure downstream of valve for V60.3. Calculated results are shown with triangles.

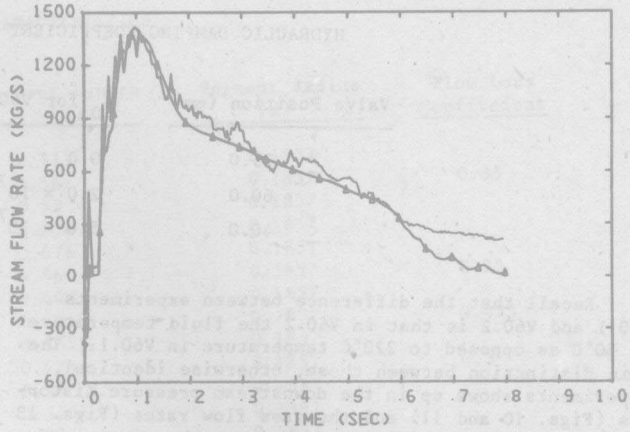

Fig. 13. Mass flow rate at measuring ring I for V60.1. Calculated results are shown with triangles.

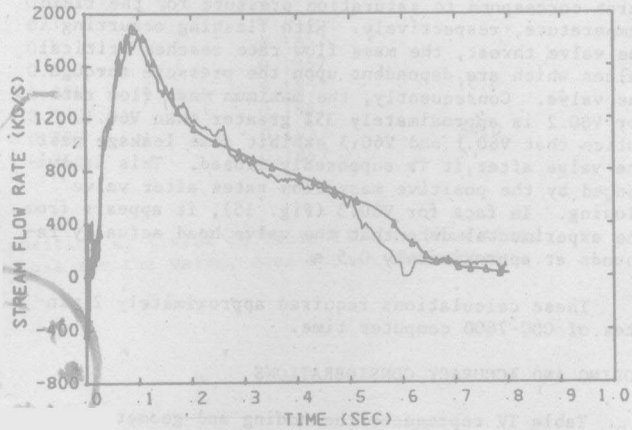

Fig. 14. Mass flow rate at measuring ring I for V60.2. Calculated results are shown with triangles.

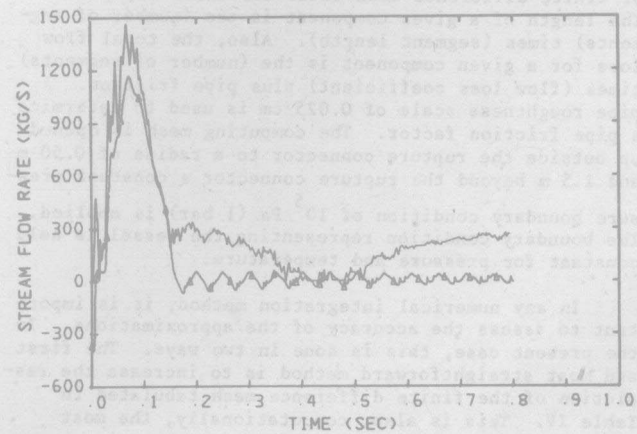

Fig. 15. Mass flow rate at measuring ring I for V60.3. Calculated results are shown with triangles.

TABLE III

HYDRAULIC DAMPING COEFFICIENT AS A FUNCTION OF VALVE POSITION

Valve Position (mm)	C_D for V60.1	C_D for V60.2	C_D for V60.3
$\geq$ 75.0	0.0	0.0	0.0
60.0	2.0×10^7	2.0×10^7	1.0×10^6
$\leq$ 40.0	5.0×10^7	5.4×10^7	1.0×10^6

Recall that the difference between experiments V60.1 and V60.2 is that in V60.2 the fluid temperature is 50°C as opposed to 220°C temperature in V60.1. The main distinction between these, otherwise identical, experiments shows up in the downstream pressure histories (Figs. 10 and 11) and the mass flow rates (Figs. 13 and 14). After the initial transient, the pressure for V60.1 is about 2.3×10^6 Pa (23 bar) as contrasted to roughly 1.2×10^4 Pa (0.12 bar) for V60.2. These pressures correspond to saturation pressure for the fluid temperature, respectively. With flashing occurring in the valve throat, the mass flow rate reaches critical values which are dependent upon the pressure through the valve. Consequently, the maximum mass flow rate for V60.2 is approximately 35% greater than V60.1. Notice that V60.1 and V60.3 exhibit some leakage past the valve after it is supposedly closed. This is evidenced by the positive mass flow rates after valve closing. In fact for V60.3 (Fig. 15), it appears from the experimental data that the valve head actually rebounds at approximately 0.5 s.

These calculations required approximately 2 minutes of CDC-7600 computer time.

NODING AND ACCURACY CONSIDERATIONS

Table IV represents the noding and geometric characteristics of the pipe system used in the above calculations. The components refer to Fig. 1, while the number of segments in each component defines the number of finite-difference mesh cells for that component. The length of a given component is the (number of segments) times (segment length). Also, the total flow loss for a given component is the (number of segments) times (flow loss coefficient) plus pipe friction. A pipe roughtness scale of 0.025 cm is used to determine a pipe friction factor. The computing mesh is opened up outside the rupture connector to a radius of 0.50 m and 1.5 m beyond the rupture connector a constant pressure boundary condition of 10^5 Pa (1 bar) is applied. The boundary condition representing the vessel is held constant for pressure and temperature.

In any numerical integration method, it is important to assess the accuracy of the approximations. In the present case, this is done in two ways. The first and most straightforward method is to increase the resolution of the finite difference mesh tabulated in Table IV. This is also, computationally, the most costly method. In the SOLA-LOOP code, there is a second, more efficient method to check errors induced by numerical diffusion. All convective flux terms in the SOLA-LOOP code are approximated by a mixture of centered and upstream or donor cell finite difference expressions. The mixture is controlled by an input parameter ALPHA, such that a value of unity for ALPHA results in donor cell differencing, while a zero value corresponds to centered differencing. For numerical stability, it is generally necessary that ALPHA remain greater than the largest value of $|u|\delta t/\delta y$ occurring in the mesh. However, the closer ALPHA is to this stability limit, the smaller will be the numerical diffusion. Both of these accuracy checks have been incorporated in developing confidence in the numerical solution. The final mesh configuration, as listed in Table IV, was determined after applying mesh refinements and setting ALPHA close to the stability limit with the resulting effect being only small changes in the solution.

CONCLUSIONS

It has been demonstrated that the coupling of numerical tools, such as SOLA-LOOP and a model for the dynamic behavior of a back-pressure check valve, is a significant calculation aid for designing complex network system components in order to achieve near optimum performance characteristics. Calculated results are seen to be in excellent agreement with the overall experimental data and in remarkably good agreement with the fine structure and features of the measured quantities.

ACKNOWLEDGEMENTS

The authors wish to express their appreciation for discussions with F. H. Harlow. This work was supported by the United States Nuclear Regulatory Commission, Division of Reactor Safety Research, Washington, DC.

REFERENCES

1. "Investigations of Feed-Water Back-Pressure Valve NW350 upon Breakage of a Reactor Coolant Medium Pipe, Quick Look Report, SRV350," Techn. Fachbericht PHDR 11-80 (April 1980).

2. C. W. Hirt, T. A. Oliphant, W. C. Rivard, N. C. Romero, and M. D. Torrey, "SOLA-LOOP: A Nonequilibrium, Drift-Flux Code for Two-Phase Flow in Networks," Los Alamos National Laboratory report LA-7659 (June 1979).

3. F. H. Harlow and A. A. Amsden, "A Numerical Fluid Dynamics Calculation Method for All Flow Speeds," J. Comput. Phys. 8, 197 (1971).

4. T. Grillenberger, "German Standard Problem No. 4: Breakage of a Feed-Water Pipe with a Back-Pressure Valve, Specification," June 1980.

5. J. W. Daily, W. L. Hankey, Jr., R. W. Olive, and J. M. Jordaan, Jr., "Resistance Coefficients for Accelerated and Decelerated Flows Through Smooth Tubes and Orifices," Trans. ASME, 78, No. 5, pp. 1071 (July 1956).

TABLE IV

PIPE SYSTEM CHARACTERISTICS

Component	Number of Segments	Segment Length (m)	Segment Radius (m)	Flow Loss Coefficient
T-connector	1	0.517	0.1857	
+ RPT	2	0.56	0.1857	0.35
Pipe Section	1	0.52	0.1857	
30° elbow	2	0.656	0.1857	
Pipe Section	1	0.676	0.1857	
60° elbow	1	0.56	0.1857	0.35
Pipe Section	3	0.498	0.1857	
90° elbow	2	0.42	0.1857	0.475
Pipe Section	10	0.4655	0.1857	
90° elbow	2	0.4785	0.1857	0.3
Pipe Section	3	0.33	0.1857	
SRV 350	4	0.3125	0.1857	*
Pipe Section	2	0.35	0.1857	
61° elbow	2	0.324	0.1857	0.175
T-fitting	1	0.32	0.199	
	3	0.3714	0.214	
Pipe End Section	4	0.28145	0.2265	
S-Loop Pipe Section	30	0.35	0.1857	
Slow Closing Valve	2	0.35	0.1857	
Pipe Section	12	0.360	0.1857	
Pump	1	0.350	0.1857	10.0
Pipe Section	6	0.377	0.1857	
Fast Closing Valve	1	0.300	0.1857	30.0
Pipe Section	9	0.366	0.1857	

* Flow loss coefficient as a function of valve position as listed in Table II. In this case, Table II plus pipe friction is the total flow loss for the valve, even though the experimental valve is represented by four segments.

PRESSURE LOSSES THROUGH OBSTRUCTION IN BOTH HORIZONTAL AND VERTICAL BUBBLY FLOWS

M. E. Salcudean and L. K. H. Leung
Department of Mechanical Engineering
University of Ottawa
Ottawa, Ontario, Canada

ABSTRACT

Two-phase pressure drops in both adiabatic vertical and horizontal bubbly flows have been determined in the presence of flow blockages. The pressure drops due to friction and obstruction have been determined based on pressure data obtained with a Meriam 33KB35 multi-tube well-type manometer.

The results have indicated that the local pressure drop due to obstruction is affected by both the size and the location of the blockage. A larger pressure drop is observed for an obstruction interfering with a higher velocity mixture. The stratification occurring in horizontal bubbly flow affects the pressure drop but its influence is less than in annular flow.

NOMENCLATURE

B = coefficient in eqn. 2

G = mass flux, kg/m^2-s

g = acceleration due to gravity, m/s^2

K = head loss coefficient

v = velocity, m/s

x = mass quality

Greek

α = void fraction

$\frac{dP}{dz}$ = pressure drop, kPa/m

μ = dynamic viscosity, kg/m-s

ρ = density, kg/m^3

θ = angle between channel axis and horizontals

ΔP = local pressure drop, kPa

Subscript

A = due to acceleration

G = due to gravity

g = gas phase

LO = with total single phase flow as liquid

ℓ = liquid phase

SP = due to obstruction in single-phase flow

TP = two-phase flow

INTRODUCTION

Two-phase flow in which the light phase is dispersed as bubbles in the heavy phase is known as "bubbly flow". It occurs in many two-phase systems at low qualities. The presence of the second phase influences the pressure drop and heat transfer in the system. The two-phase pressure drop is due to acceleration, gravity, and friction and depends on the flow parameters. The frictional pressure drop is generally expressed as a two-phase multiplier, which relates the pressure drop occurring in two-phase flow to the single phase pressure drop and was first introduced by Lockhart and Martinelli (1). The two-phase multiplier is written as

$$\phi^2_{LO} = \left(\frac{dP}{dz}\right)_{TP} / \left(\frac{dP}{dz}\right)_{LO} \qquad (1)$$

Systematic correlations, such as the ones by Lockhart & Martinelli (1) and Baroczy (2), have been determined for predicting the frictional pressure drop in various two-phase flows. Two-phase multipliers were also expressed as equations through a theoretical approach by Chisholm (3,4). Beattie has predicted two-phase pressure drops using a mixing length model (5). The predictions are in reasonable agreement with the experimental data for bubbly flow obtained by Richardson (6). In vertical

flow, the two-phase pressure drop has been studied for various flow patterns by Govier et al. (7). The results indicate a pressure drop dependence on the flow patterns. Orkiszewski (8) presented a flow pattern dependent estimation method, which was also discussed and recommended by DeGance and Atherton (9). A general correlation, which can be applied without the knowledge of flow patterns, has been proposed by Hughmark and Pressburg (10). The pipe inclination effect on pressure drop has been investigated by Chisholm (11). He has found that the pressure drop is larger in vertical flows than in horizontal flows. In his conclusions, he proposed two different equations for its representation. Variations of pressure drop in both horizontal and vertical annular flows have been investigated recently by Salcudean & Leung (12). It was found that the equations recommended by Chisholm predict the experimental results fairly well.

Two-phase flow multipliers relating the pressure drop through the obstructions to the single-phase local pressure drop are extensively used. The homogeneous two-phase multiplier[1] was widely used for orifices (13) since homogeneous mixtures had been observed after the obstruction by several researchers. Chisholm (13) proposed a general equation with variable coefficient B, to estimate the pressure drops through different obstructions. The equation is written as

$$\phi^2_{LO} = 1 + (\rho_\ell/\rho_g - 1)(B \times (1 - x) + x^2) \qquad (2)$$

For both vertical and horizontal annular flows, the effect of obstruction with different sizes, shapes, and locations has been investigated recently (12,15). It was concluded that the local pressure drop due to the obstruction depends strongly on both the size and the location of the obstruction. Although the flow stratification effect decreases with the increase of the gas flow rate, it is nevertheless significant. The local pressure loss is larger for obstructions intercepting the mixture with higher momentum and kinetic energy. The research has been extended to both vertical and horizontal bubbly flows and the results are presented in the present work.

EXPERIMENTAL SET-UP

Two air-water loops (Figure 1 shows the set-up for vertical flow) have been built for the present investigation. The flow rates of the working fluid, which were controlled with gate valves, were measured with rotameters of various ranges. Before entering the test-section, the two streams were mixed with a spray type mixer. After the mixer, a calming section was introduced to stabilize the mixture. Two pieces of copper pipe, each 0.0254-m in diameter, 1.83-m long, were used as test-section. They were connected with two pieces of flange, each of which was soldered to one end of the pipe. The obstruction plate was inserted in between the flanges. Local pressures at various positions were measured with a Meriam 33KB35 multi-tube manometer through pressure tappings brazed along the test-section. The manometric fluid used was acetylene tetrabromide; specific gravity 2.95. The static pressure was evaluated from the difference in pressure between the tap location and the reference pressure reservoir connected to a reference pressure tap. The static pressure at the reference tap was measured with a Bourdon pressure gauge.

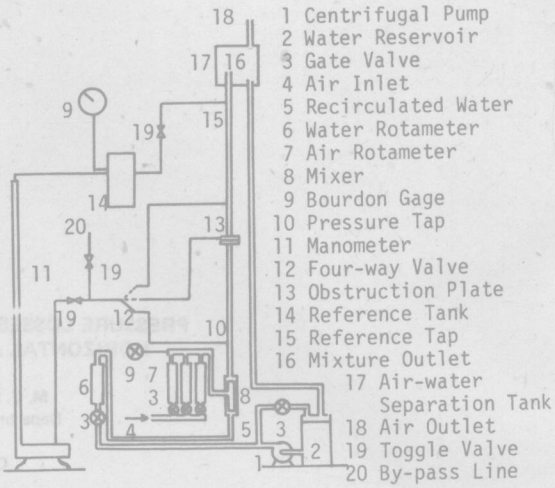

Fig. 1 Schematic diagram of the vertical loop.

Toggle valves that could be closed simultaneously were installed for recording the height of the manometric fluid. Bypass lines were provided to remove air bubbles from connecting lines between the manometer and the pressure tappings. Similar static pressure at the obstruction between horizontal and vertical flow was achieved by adjusting the gate valve installed at the exit of the test-section.

Four different shapes of obstruction plates (see Figure 2), with blockage area ratios[2] of 25% and 40% were tested. The central segment obstruction and the peripheral segment obstruction were placed at different positions in the horizontal flow to study the effect of flow stratification. The central segment obstruction was arranged either horizontally or vertically in the channel, while the peripheral segment obstruction was placed to block either the top or the bottom of the channel.

RESULT AND DISCUSSION

Single-phase Flow

The pressure drops for single-phase flow (water only) have been measured for Reynolds number varying between 10000 and 200000. At large Reynolds number, the average friction factor for the channel has been found to be 0.0148. The single-phase local pressure drop due to obstruction presented as head loss coefficient is shown in Table 1. The head loss coefficient, K, is defined as

$$K = 2\left(\frac{\Delta P}{SP}\right)/(\rho_\ell v_\ell^2) \qquad (4)$$

Two-phase Pressure Drops

Two-phase pressure drops are presented for air mass flow rates ranging from 0.0002 to 0.0061 kg/s with a constant water mass flow rate of 1.6 kg/s. The water mass flow rate corresponds to a Reynolds number of approximately 83000. The flow patterns involved, which are determined with the flow pattern maps published by Salcudean et al. (16) for horizontal flow and by Hewitt & Roberts (17) for vertical flow, are mainly bubbly flow with transition to slug or wispy annular flow. Salcudean et al. (16) have investigated the flow transition with an experimental set-up similar to the one used in the present

[1] The homogeneous two-phase multiplier is written as

$$\phi^2_{LO} = (1 + x(\rho_\ell/\rho_g - 1)(1 + x(\mu_\ell/\mu_g - 1))^{-0.25} \qquad (3)$$

[2] The blockage area ratio is defined as the percentage of channel cross-sectional area occupied by the obstruction.